Mon. Not. R. Astron. Soc. **000**, 1–12 (2015) Printed 24 September 2015 (MN LATEX style file v2.2)

The distribution function of the Galaxy's dark halo

J. Binney⋆ and T. Piffl
Rudolf Peierls Centre for Theoretical Physics, Keble Road, Oxford OX1 3NP, UK

arXiv:1509.06877v1 [astro-ph.GA] 23 Sep 2015

Draft, 24 September 2015

ABSTRACT

Starting from the hypothesis that the Galaxy's dark halo responded adiabatically to the infall of baryons, we have constructed a self-consistent dynamical model of the Galaxy that satisfies a large number of observations, including measurements of gas terminal velocities and masers, the kinematics of a 180 000 giant stars from the RAVE survey, and star count data from the SDSS. The stellar disc and the dark halo are both specified by distribution functions (DFs) of the action integrals. The model is obtained by extending the work of Piffl, Penoyre & Binney from the construction of a single model to a systematic search of model space. Whereas the model of Piffl, Penoyre & Binney violated constraints on the terminal-velocity curve, our model respects these constraints by adopting a long scale length $R_{\rm d} = 3.66\,$kpc for the thin and thick discs. The model is, however, inconsistent with the measured optical depth for microlensing of bulge stars because it attributes too large a fraction of the density at $R \lesssim 3\,$kpc to dark matter rather than stars. Moreover, it now seems likely that the thick disc's scale-length is significantly shorter than the model implies. Shortening this scale-length would cause the constraints from the rotation curve to be violated anew. We conclude that we can now rule out adiabatic compression of our Galaxy's dark halo.

Key words: dark matter – galaxies: haloes – solar neighbourhood – Galaxy: disc – Galaxy: fundamental parameters – Galaxy: halo

1 INTRODUCTION

Over the coming decade models of our Galaxy will play a crucial role in the extraction of physical understanding from the data that are currently being collected by a series of large surveys (e.g. Binney 2011). The models of choice are fully dynamical in the sense that they take full account of the equations of motion of the Galaxy's constituent particles and of the laws of gravitation.

An important class of such models represent the Galaxy by a large number of particles. The model is then specified by the phase-space coordinates, masses and other properties of the particles. Specifications of this kind are highly redundant in the sense that on integrating the equations of motion for a dynamically insignificant time, such as 10 Myr, all the phase-space coordinates change while the model remains the same. This redundancy is associated with great complexity in the sense that millions of particles are required to achieve even mediocre spatial resolution in the model, so (a) at least 10 million real numbers are required to specify a model, and (b) given these numbers it is a totally non-trivial exercise to characterise the model in a meaningful way. Moreover, as a consequence of this complexity, the models are typically computationally expensive to produce and it is unlikely to prove feasible to fit such a model to the wide range of very detailed data for our Galaxy that are becoming available.

Models of a very different class are specified by a distribution function (DF) $f_\alpha(\mathbf{J})$ for each population α of constituent particles. Each DF is an analytic function of three constants of orbital motion, which it is convenient to choose to be the actions J_i, and specifies the probability density of particles of type α in the three-dimensional region of phase space associated with a given set $\mathbf{J}$ of action values. The legitimacy of assuming that DFs depend only on $\mathbf{J}$ is assured by Jeans' theorem (Binney & Tremaine 2008). The model is specified by giving the values of the parameters $\mathbf{p}$ that appear f_α alongside the actions. Hence the model is specified by the values of $\lesssim 100$ numbers, rather than millions, and it is computationally feasible to adjust the parameters to optimise the agreement between the model and the data. Moreover, the parameters can be chosen to be approximately equal to intuitive properties of the population, such as its radial scale length, radial and vertical velocity dispersions in the solar neighbourhood, etc.

In a series of papers Binney (2010, 2012); Binney et al. (2014); Piffl et al. (2014) we have demonstrated the effectiveness of a particular form of DF for disc stars. Binney (2012) fitted this DF to the kinematics of stars in the Geneva-Copenhagen Survey (Nordström et al. 2004; Holm-

⋆ E-mail: binney@physics.ox.ac.uk

© 2015 RAS

berg et al. 2007; Casagrande et al. 2011, hereafter GCS), which lie within $\sim 120\,$pc of the Sun. The resulting model was then used to predict the kinematics of stars in the RAdial Velocity Experiment (Steinmetz et al. 2006; Kordopatis et al. 2013, hereafter RAVE), which extend to $\sim 2.5\,$kpc of the Sun (Binney et al. 2014). The ability of the model to reproduce data very different from that used in the model's specification is remarkable in view of the limited extent to which the thick disc contributes to the GCS data. Piffl et al. (2014, hereafter P14) showed that minor adjustments to the parameter values in Binney (2012) enabled the model to fit simultaneously the RAVE data and data from the Sloan Digital Sky Survey in Jurić et al. (2008, hereafter J08), and yielded the currently strongest constraints on the mass of dark matter within the solar radius, R_0.

Fundamentally stars form a multi-dimensional continuum spanned by mass, age, and chemistry. Models need to take cognisance of the masses, ages and chemical compositions of stars because these intrinsic variables determine a star's absolute magnitudes in the various observing bands, and thus the probability that a star will be included in any given data set. The work summarised above handled these complexities very crudely by supposing that our Galaxy comprises a continuum of stellar populations that differ only in age. Even within this rough approximation the analysis was unnecessarily crude. Sanders & Binney (2015) moved the use of analytic DFs to a new level of sophistication by (a) introducing metallicity [Fe/H] as an argument of the DF of disc stars, and (b) using isochrones to compute the number of stars the model predicts will be observed in given surveys. Sanders & Binney (2015) fitted their "extended DF" for the disc to the GCS and compared the resulting predictions for the more distant G dwarfs in the Sloan Extension for Galactic Understanding and Exploration (Yanny et al. 2009, hereafter SEGUE).

Although much remains to be done, as a result of the work just summarised, we now have a reasonable understanding of the phase-space distribution of disc stars – the extensions that seem most urgent are to compare the model's predictions with data for stars that never come close to the Sun, and to model the way non-stationary features such as the Galactic bar and spiral structure modify the model's static DF.

Our Galaxy is by no means comprised of just stars: overall more than 90 percent of its mass is thought to be contributed by dark-matter particles, and from the RAVE data using an analytic DF for the disc, P14 concluded that even interior to the Sun, where baryons make their largest contribution to the overall mass, more than half the matter is dark.

In the work with analytic DFs so far mentioned, dark matter was included merely by adding to the gravitational field generated by stars and gas a hypothetical contribution from the dark halo. The density distribution of the dark halo that was used by P14 and similar studies was inspired by simulations of cosmological clustering that did not include baryons, and hence side-stepped the complex physics that baryons bring into play. In these simulations the density profiles of dark halos are well approximated by a simple functional form, the so-called NFW profile, regardless of the mass or assembly histories of individual halos (Navarro et al. 1997). Given that we have yet to actually detect any dark-matter particles, and dark matter strongly dominates the Galaxy's overall mass budget, real dark halos are widely modelled as spherical or mildly spheroidal version of the profile.

The intellectual basis for this procedure is weak, however, because even if a given dark halo conformed to the NFW profile before the bulk of the baryons flowed in and formed stars, it would be a remarkable coincidence if it conformed to this profile now. Indeed, if the baryons accumulated over many dynamical times rather than in a few massive infall events then the actions of the dark-matter particles will be invariant as the Galaxy grows, and it will be the DF of the dark matter, not its spatial density profile, which will be invariant. The existence of an old thin disc favours the hypothesis that baryons accumulate quiescently.

This line of argument motivated (Piffl et al. 2015, hereafter PPB) to open a new chapter in the use of analytic DFs by specifying the dark halo through its DF rather than its spatial density distribution. Hence the Galaxy model they fitted to RAVE data was based on analytic DFs for both the stars and the dark matter, and the spatial distributions of these components were determined by iteratively solving for the gravitational potential that these components jointly generate in concert with smaller, specified contributions from gas and an axisymmetrised version of the Galactic bulge/bar. PPB took as their point of departure the model P14 had fitted to RAVE and J08 data. This model provided the complete DF of the disc and a particular NFW profile. PPB adopted the disc DF, and for the DF of the dark halo used one that self-consistently generates the given NFW profile *in the absence of the disc*. PPB found that when this dark halo cohabits with the disc, the disc's gravitational field contracts the central portion of the dark halo sufficiently to cause the final model to be inconsistent with the measured circular speed v_c at $R \lesssim 6\,$kpc.

This conflict between data and the first model of our Galaxy to specify the dark halo through its DF, can be addressed in two extreme ways: one can modify the DF of either the disc or the dark halo, leaving the other alone. Modification of the halo's DF would imply that the infall of baryons was sufficiently unsteady to violate adiabatic invariance of the actions of halo particles. Here we ask whether this conclusion can be avoided by leaving the functional form of the dark halo's DF alone and seeking a disc DF that is consistent with the observational data when the disc cohabits with a dark halo of this form, and the previously assumed quantities of gas and bulge stars. We will show that with current data it is possible to model the RAVE and SEGUE data successfully within constraints set by measurements of v_c by increasing the scale length of the disc from $\sim 2.5\,$kpc to $\sim 3.5\,$kpc, but find that the resulting model then predicts too little microlensing of bulge stars.

A key achievement of this paper is the development of a practical technique for searching a multi-dimensional model space for a model that satisfies observational constraints on the space density and kinematics of stars in the extended solar neighbourhood, and constraints from gas, masers and Sgr A* on the Galaxy's rotation curve. In forthcoming work we plan to use this technique to obtain fully dynamical models of our Galaxy that are consistent with all available observations.

In Section 2 we list our observational inputs. In Sec-

tion 3 we specify the functional forms that define our models. In Section 4 we explain how we fit the data. Section 5 describes the best-fit model. Section 6 discusses the implications of the model and in Section 7 we sum up and draw conclusions.

2 OBSERVATIONAL INPUTS

We use the same observations as in P14, apart from dropping the constraints for the dark halo. We assume a distance of the Sun to the Galactic centre (GC), R_0, to be 8.3 kpc (e.g. Gillessen et al. 2009; McMillan 2011; Schönrich 2012), the distance of the Sun above the Galactic plane, z_0, to be 14 pc (Binney et al. 1997) and the solar motion with respect to the local standard-of-rest (LSR), $\mathbf{v}_\odot$, to be $(11.1, 12.24, 7.25)\,\mathrm{km\,s^{-1}}$ (Schönrich et al. 2010).

Our most important inputs are (i) the vertical profile of stellar density above the Sun determined by J08, and (ii) the kinematics of $\sim 180\,000$ giant stars in RAVE.

2.1 Vertical density profile from SDSS

We assume that the population from which the RAVE sample is drawn is identical to that studied by J08, who measured its vertical density profile by means of a main-sequence colour-magnitude relation. We use the data points shown in the middle panel of their Figure 15, which shows results from M dwarf stars in the colour range $0.70 < r - i < 0.80$. Similar to RAVE, this sample should carry only weak biases in metallicity and age. Rather than correcting the data for the effects of Malmquist bias and binarity as J08 did, P14 imposed these effects on the model. Since this step had a negligible effect on their results, we omitted it.

We decomposed the J08 density profile into contributions from the disc and stellar halo. This decomposition implied that at $(R, z) = (R_0, 0.5\,\mathrm{kpc})$, the density of the stellar halo is 0.0056 times the density of the disc. The DF of the stellar halo is subsequently always normalised to produce this ratio of densities at $(R_0, 0.5\,\mathrm{kpc})$.

2.2 Kinematics from RAVE

For the kinematics we use the stellar parameters and distance estimates in the fourth RAVE data release (Kordopatis et al. 2013). We define eight spatial bins in the (R, z) plane. Four bins for stars inside the solar cylinder with $R_0 - 1\,\mathrm{kpc} < R < R_0$ and $|z|$ in [0,0.3],[0.3,0.6],[0.6,1.0] or [1,1.5] kpc. The other four bins cover the same z ranges but cover the regions 1 kpc outside the solar cylinder, i.e. $R_0 < R < R_0 + 1\,\mathrm{kpc}$. After sorting the stars into these bins, we compute the velocity distributions predicted by the DF at the mean (R, z) positions (barycentre) of the stars in each bin. For each bin we have a histogram for each component of velocity, so we accumulate χ^2 from 24 histograms. Throughout this work we compute velocities in the coordinate system that Binney et al. (2014) found to be closely aligned with the velocity ellipsoid throughout the extended solar neighbourhood – this system is quite closely aligned with spherical coordinates. We denote the velocity component along the long axis of the velocity ellipsoid – pointing more or less towards the Galactic centre – with V_1, the azimuthal component with V_ϕ, and the remaining component with V_3.

The resulting model distributions cannot be directly compared to the observed distributions, because the latter are widened by errors in the velocity and parallax estimates. We fold the model distributions with the average velocity uncertainties of the bin's stars to obtain $N_{\mathrm{bary}}(V_i)$. The distortions arising from the parallax error are less straight forward to introduce: following Binney et al. (2014) we create a Monte Carlo realisation of a given DF by randomly assigning to each star in our RAVE sample a new "true" distance according to its (sometimes multi-modal) distance pdf, and a new "true" velocity according to the model velocity distribution at this position. With these new phase space coordinates we compute new observed line-of-sight velocities and proper motions. These are finally equipped with random observational errors. Using the original catalogue distances, we then compute new realistically distorted velocity distributions, $N_{\mathrm{MC}}(V_i)$, based on the DF that can be compared directly to the original RAVE distributions in a number of spatial bins. We minimise the Poisson noise in $N_{\mathrm{MC}}(V_i)$ by choosing 100 new velocities for each star. This procedure is computationally expensive and the distortions vary only weakly for reasonable choices of the DF parameters. To speed up the process, we store the ratio $N_{\mathrm{bary}}(V_i)/N_{\mathrm{MC}}(V_i)$ for a DF that is already a good match of the RAVE data. Examples of these ratios, which are near unity in the core of the distribution but fall to < 0.2 in the wings, are shown in the lower panels of Fig. 4 of P14. These ratios are then used to correct all DF predictions before they are compared with the data.

Our model selection involves computing the corresponding velocity histograms at the barycentre of each bin, and optimising the fit between the data and these histograms after the latter have been modified to allow for the impact of errors in the measurements of velocity and distance.

2.3 Gas terminal velocities

The distribution of HI and CO emission in the longitude-velocity plane yield a characteristic maximum ("terminal") velocity for each line of sight (e.g. Binney & Merrifield 1998, §9.1.1). The terminal velocities are related to the circular speed $v_{\mathrm{c}}(R)$ by

$$\begin{aligned} v_{\mathrm{term}}(l) &= v_{\mathrm{c}}(R) - v_{\mathrm{c}}(R_0)\sin l \\ &= v_{\mathrm{c}}(R_0\sin l) - v_{\mathrm{c}}(R_0)\sin l. \end{aligned} \tag{1}$$

We use the terminal velocities $v_{\mathrm{term}}(l)$ from Malhotra (1995). Following Dehnen & Binney (1998) and McMillan (2011) we neglect data at $\sin l < 0.5$ in order not to be influenced by the Galactic bar, and we assume that the ISM has a Gaussian velocity distribution of dispersion $7\,\mathrm{km\,s^{-1}}$.

2.4 Maser observations

Reid et al. (2014) presented a compilation of 103 maser observations that provide precise 6D phase space information. Since masers are associated with young stars their motions should be very close to circular around the GC. We again assume an intrinsic velocity dispersion of $7\,\mathrm{km\,s^{-1}}$ and no lag

against the circular speed (van der Kruit & Shostak 1984; McMillan & Binney 2010). For the likelihood computation we neglected 15 sources that were flagged as outliers by Reid et al. (2014) and also all sources at $R < 4\,\mathrm{kpc}$. The latter is again to prevent a bias by the Galactic bar. To assess the likelihood of a maser observation, we predict the observed velocities (line-of-sight velocity, proper motions) as functions of heliocentric distance and then integrate the resulting probability density along the line-of-sight.

2.5 Proper motion of SgrA*

Reid & Brunthaler (2004) measured the proper motion of the radio source SgrA* in the GC to be

$$\mu_{\mathrm{SgrA}^\star} = -6.379 \pm 0.024\ \mathrm{mas\,yr}^{-1}. \quad (2)$$

This source is thought to be associated with the supermassive black hole that sits in the gravitational centre of the Milky Way with a peculiar velocity below $1\,\mathrm{km\,s}^{-1}$. Hence this measurement reflects the solar motion with respect to the GC.

3 MODEL DEFINITIONS

3.1 The stellar disc

The functional form of the stellar disc's DF, which is made up of contributions from the thick disc and each coeval cohort of thin-disc stars, is unchanged from PPB, even though Sanders & Binney (2015) have strictly speaking rendered that form obsolete. The DF segments the disc by age: the oldest stars are represented by a DF for the "thick disc". The thick disc's DF is a "quasi-isothermal" component (Binney & McMillan 2011). The DF of such a component is

$$f(J_r, J_z, L_z) = f_{\sigma_r}(J_r, L_z) f_{\sigma_z}(J_z, L_z), \quad (3)$$

where f_{σ_r} and f_{σ_z} are defined to be

$$f_{\sigma_r}(J_r, L_z) \equiv \frac{\Omega\Sigma}{\pi\sigma_r^2\kappa}[1 + \tanh(L_z/L_0)]\mathrm{e}^{-\kappa J_r/\sigma_r^2} \quad (4)$$

and

$$f_{\sigma_z}(J_z, L_z) \equiv \frac{\nu}{2\pi\sigma_z^2}\,\mathrm{e}^{-\nu J_z/\sigma_z^2}. \quad (5)$$

Here $\Omega(L_z)$, $\kappa(L_z)$ and $\nu(L_z)$ are, respectively, the circular, radial and vertical epicycle frequencies of the circular orbit with angular momentum L_z, while

$$\Sigma(L_z) = \Sigma_0 \mathrm{e}^{-R_\mathrm{c}/R_\mathrm{d}}, \quad (6)$$

where $R_\mathrm{c}(L_z)$ is the radius of the circular orbit, determines the surface density of the disc: to a moderate approximation the surface density at Galactocentric distance R can be obtained by using for L_z in equation (6) the angular momentum $L_z(R)$ of the circular orbit with radius R.

In equation (4) the factor containing tanh serves to eliminate retrograde stars; the value of L_0 controls the radius within which significant numbers of retrograde stars are found, and should be no larger than the circular angular momentum at the half-light radius of the bulge/bar. Provided this condition is satisfied, the results for the extended solar neighbourhood presented here are essentially independent of L_0.

The DF of the thin disc is taken to be a superposition of quasi-isothermal DFs, one for the stars of each age τ. The velocity-dispersion parameters σ_r and σ_z above are functions $\sigma_r(L_z, \tau)$ and $\sigma_z(L_z, \tau)$ of angular momentum and age. They control the radial and vertical velocity dispersions of the stars of age τ and are approximately equal to them at R_c. Given that the scale heights of galactic discs do not vary strongly with radius (van der Kruit & Searle 1981), these quantities must increase inwards, and we assume this dependence on R_c is exponential. We take the growth with age of the velocity dispersions of a coeval cohort of thin-disc stars from the work of Aumer & Binney (2009). With these assumptions the velocity-dispersion parameters are given by

$$\sigma_r(L_z, \tau) = \sigma_{r0}\left(\frac{\tau + \tau_1}{\tau_\mathrm{m} + \tau_1}\right)^\beta \mathrm{e}^{(R_0 - R_\mathrm{c})/R_{\sigma,r}}$$
$$\sigma_z(L_z, \tau) = \sigma_{z0}\left(\frac{\tau + \tau_1}{\tau_\mathrm{m} + \tau_1}\right)^\beta \mathrm{e}^{(R_0 - R_\mathrm{c})/R_{\sigma,z}}. \quad (7)$$

Here σ_{z0} is the approximate vertical velocity dispersion of local stars at age $\tau_\mathrm{m} \simeq 10\,\mathrm{Gyr}$, τ_1 sets velocity dispersion at birth, and $\beta \simeq 0.33$ is an index that determines how the velocity dispersions grow with age. The radial scale-lengths on which the velocity dispersions decline are $R_{\sigma,i}$, and a constant scale height would be follow if $R_{\sigma,z} \sim 2R_\mathrm{d}$.

We assume that the star-formation rate in the thin disc has decreased exponentially with time, with characteristic time scale t_0, so the thin-disc DF is

$$f_\mathrm{thn}(J_r, J_z, L_z) = \frac{\int_0^{\tau_\mathrm{m}} \mathrm{d}\tau\, \mathrm{e}^{\tau/t_0} f_{\sigma_r}(J_r, L_z) f_{\sigma_z}(J_z, L_z)}{t_0(\mathrm{e}^{\tau_\mathrm{m}/t_0} - 1)}, \quad (8)$$

where σ_r and σ_z depend on L_z and τ through equation (7). We set the normalising constant Σ_0 that appears in equation (6) to be the same for both discs and use for the complete DF

$$f_\mathrm{disc}(J_r, J_z, L_z) = f_\mathrm{thn}(J_r, J_z, L_z) + F_\mathrm{thk} f_\mathrm{thk}(J_r, J_z, L_z), \quad (9)$$

where F_thk is a parameter that controls the fraction $(1 + F_\mathrm{thk}^{-1})^{-1}$ of stars that belong to the thick disc. The values of the parameters for our final model are given in Table 2.

We followed PPB in imposing a lower limit of $1\,\mathrm{kpc}$ on the value of $R_\mathrm{c}(J_\phi)$ at which the epicycle frequencies $\kappa(J_\phi)$ and $\nu(J_\phi)$ are evaluated for use in the DF.

3.2 DF of the stellar halo

As in P14, we include the contribution of a stellar halo when fitting the kinematics of RAVE stars, which include a small but non-negligible population of stars that are identifiable as halo stars by their low or even negative values of the azimuthal velocity v_ϕ. Including the DF of the stellar halo prevents the fitting routine distorting the thick disc in an attempt to account for the presence of halo stars in the sample.

The density of the stellar halo is generally thought to follow a power-law in Galactocentric radius, i.e. $\rho_\mathrm{halo} \propto r^{-\alpha}$, with the power-law index $\alpha \simeq 3.5$ (e.g. Binney & Merrifield 1998, §10.5.2). We can model such a configuration using the following form of the (un-normalised) DF (Posti et al. 2015)

$$f(\mathbf{J}) = g(\mathbf{J})^{3.5} \exp\{-[g(\mathbf{J})/g_\mathrm{max}]^4\}, \quad (10)$$

where

$$g(\mathbf{J}) \equiv J_r + \gamma_1|L_z| + \gamma_2 J_z + J_{\rm core}^{(\rm s)} \tag{11}$$

with $\gamma_1 = 0.937$, $\gamma_2 = 0.682$, $J_{\rm core}^{(\rm s)} = 200\,{\rm km\,s^{-1}\,kpc}$ and $g_{\rm max} = 2.5\times10^5\,{\rm km\,s^{-1}\,kpc}$. These choices of γ_1 and γ_2 make the stellar halo approximately spherical. The RAVE data alone are not well suited to constraining the stellar halo, so we defer this exercise to a later paper (Das & Binney in preparation). We include the stellar halo only to prevent distortion of the thick disc that is fitted to the data. Our complete total stellar DF is

$$f(J_r,J_z,L_z) = f_{\rm disc}(J_r,J_z,L_z) + F_{\rm halo} f_{\rm halo}(J_r,J_z,L_z) \tag{12}$$

with $F_{\rm halo}$ chosen so $\rho_{\rm halo}/\rho_{\rm disc} = 0.0056$ 0.5 kpc above the Sun to be consistent with the J08 data as explained at the start of Section 2.

3.3 The dark halo

Posti et al. (2015) found a simple DF $f(\mathbf{J})$ that self-consistently generates a spherical model that has almost exactly an NFW profile. This model is essentially isotropic near its centre, and becomes mildly radially biased beyond its scale radius. PPB extended this DF so they could explore how halos with different velocity anisotropies respond to the infall of baryons. They reported results for three model dark halos, one radially biased, one tangentially biased and the original nearly isotropic model of Posti et al. Here we consider only the radially biased case, which most closely resembles the halos that form in simulations that include only dark matter. The PPB DF is defined in terms of an approximately homogeneous function of the actions

$$h(\mathbf{J}) \equiv \frac{1}{A}J_r + \frac{\Omega_\phi}{B\kappa}(|J_\phi| + J_z), \tag{13}$$

where A and B are given by equations (6) and (7) of PPB with $b = 8$ to ensure radial anisotropy:

$$\begin{aligned} A &= 4.5 + 3.5\tanh^2\left(\frac{|L_z|+J_z}{J_r+|L_z|+J_z}\right)\\ B &= 4.5 - 3.5\tanh^2\left(\frac{|L_z|+J_z}{J_r+|L_z|+J_z}\right) \end{aligned} \tag{14}$$

The quantities κ and Ω_ϕ above are epicycle and azimuthal frequencies in the self-consistent, isolated spherical model evaluated at the radius $R_{\rm c}$ of a circular orbit with angular momentum

$$J_{\rm tot} \equiv J_r + |J_\phi| + J_z. \tag{15}$$

We take the argument of $R_{\rm c}$ to be $J_{\rm tot}$ to make it an approximate function of energy, so $R_{\rm c}$ does not become small, and the epicycle frequencies large, for stars on eccentric and/or highly inclined orbits with small $|J_\phi|$.

The DF vanishes for $h > h_{\rm max} = 10^6\,{\rm km\,s^{-1}\,kpc}$, and for $h < h_{\rm max}$

$$f(\mathbf{J}) = \frac{N}{J_0^3}\frac{[1+J_0/(J_{\rm core}+h(\mathbf{J}))]^{5/3}}{[1+h(\mathbf{J})/J_0]^{2.9}} - f_{\rm tide}, \tag{16}$$

where N, J_0, $J_{\rm core}$ and $f_{\rm tide}$ are constants. The normalising constant N determines the virial mass of the dark halo, J_0 sets the radius of the transition between the inner and outer power-law segments of the system's radial density profile, $J_{\rm core} = 1.25\times10^{-2}\,{\rm km\,s^{-1}\,kpc}$ is a small number required to keep the central phase-space density finite and $f_{\rm tide}$ is chosen to make f vanish for $h = h_{\rm max} = 10^6\,{\rm km\,s^{-1}\,kpc}$. Appendix C of PPB explains the rationale for this choice of the dark halo's DF.

Once we have obtained a self-consistent model of an isolated halo, we freeze the dependence of $R_{\rm c}$ on its argument, so while we relax $\Phi_{\rm tot}$ onto the potential that is jointly generated by all the Galaxy's components, the dark halo's DF stays exactly the same function of $\mathbf{J}$. It is essential to freeze the function $f(\mathbf{J})$ during the introduction of the discs and the bulge if one seeks to learn how the halo is distorted by the gravitational fields of its companions.

Table 1. Parameters for gas disc and bulge. With the exception of Σ_0 and $R_{\rm d}$, these parameters were fixed.

Parameter	value	unit
Gas disc		
Σ_0	57.8	$\mathrm{M_\odot\,pc^{-2}}$
$R_{\rm d}$	$2R_{\rm d}$(stars)	
$z_{\rm d}$	0.04	kpc
$R_{\rm hole}$	4	kpc
$M(\infty)$	17.7×10^9	$\mathrm{M_\odot}$
$M(R_0)$	3.53×10^9	$\mathrm{M_\odot}$
Bulge		
$\rho_{0,\rm b}$	94.9	$\mathrm{M_\odot\,pc^{-3}}$
$r_{0,\rm b}$	0.075	kpc
$r_{\rm cut,b}$	2.1	kpc
$q_{\rm b}$	0.5	
$\gamma_{\rm b}$	0	
$\beta_{\rm b}$	1.8	
$M(\infty)$	8.56×10^9	$\mathrm{M_\odot}$

3.4 The bulge/bar and gas disc

Our modelling technique restricts us to axisymmetric models, so we cannot use a sophisticated model of the bulge/bar. Moreover, the data we use are only sensitive to the bulge's contribution to radial forces. Therefore we do not represent the bulge by a DF $f(\mathbf{J})$ but by a fixed axisymmetric mass distribution. Following McMillan (2011) we use a model similar to that constructed by Bissantz & Gerhard (2002).

The density distributions of the bulge is

$$\rho(R,z) = \frac{\rho_0}{m^\gamma(1+m)^{\beta-\gamma}}\exp[-(mr_0/r_{\rm cut})^2], \tag{17}$$

where

$$m(R,z) = \sqrt{(R/r_0)^2 + (z/qr_0)^2}. \tag{18}$$

Our model bulge has an axis ratio $q = 0.5$ and extends to $r_{\rm cut} = 2.1\,{\rm kpc}$: Table 1 lists all the parameters.

The gas disc is likewise represented by an axisymmetric distribution of matter that has density

$$\rho(R,z) = \frac{\Sigma_0}{2z_{\rm d}}\exp\left[-\left(\frac{R}{R_{\rm d}} + \frac{|z|}{z_{\rm d}} + \frac{R_{\rm hole}}{R}\right)\right]. \tag{19}$$

A non-zero parameter $R_{\rm hole}$ creates a central cavity in the disc. The values of the parameters are given in Table 1. The scale length $R_{\rm d}$ is set equal to twice the scale length of the stellar disc, and the surface density normalisation is

adjusted to maintain the ratio 13.5 : 35.5 between the gas and stellar surface densities at R_0 that is given in Flynn et al. (2006). R_d and Σ_0 are the only parameters that are varied: the other parameters are fixed at the values adopted by P14 and earlier investigators.

4 FITTING ALGORITHM

Since the scale action J_0 of the dark halo's DF has little bearing on the contribution of the dark halo to forces on stars in the inner Galaxy ($r \leq 10\,\mathrm{kpc}$), we fix J_0 to a value, $J_0 = 6000\,\mathrm{km\,s^{-1}\,kpc}$, consistent with values obtained in preliminary tests of a procedure that did involve varying J_0. Fixing J_0 effectively constrains the virial mass of the dark halo, so there is then no need to impose an explicit upper limit on the halo mass within 50 kpc as P14 did. With J_0 determined, the only adjustable parameter for the dark halo is its overall normalisation.

The disc DF has in principle 12 parameters: for each subdisc a mass, the normalising velocity dispersions σ_{r0} and σ_{z0}, and the radial scale lengths R_d, R_{σ_r}, R_{σ_z} of the mass density and the velocity dispersions. We reduce the free parameter count to 9 by assuming that R_d is the same for both discs, and for the thin disc setting $R_{\sigma_r} = R_{\sigma_z} = 2R_\mathrm{d}$. Since the radial range covered by RAVE increases with $|z|$, the data do contain information about the thick disc's values of R_{σ_r} and R_{σ_z}, so we let these parameters be chosen by the data. Hence the disc DF requires 9 parameters (two masses, four pseudo velocity dispersions, the radial mass scale length, two radial scale lengths for the thick disc's velocity dispersions).

When fitting to the data we have in all 10 free parameters: 9 for the stellar discs, and one for the dark halo.

The construction of a fully self-consistent model as described by PPB is computationally quite expensive because for each trial potential the density must be computed at every point of an extensive grid by integrating over all three components of velocity. Consequently, it proved impractical to go through the whole procedure in each iteration of the fitting process with in total 10 fitting parameters. To speed up the process, we exploit the fact that we already know in some detail the final mass distribution of the stellar component, because (i) our disc DF always results in a density distribution very close to a double-exponential and (ii) the star-count data from J08 set very tight constraints on the vertical structure of the disc. Hence for large parts of the fitting process we do not deal with the disc DF directly, but use a dummy potential of a double-exponential distribution with the right vertical density structure. Hence our procedure is a follows:

1. We choose a normalisation of the total mass of the dark halo.
2. We adopt a double-exponential disc that has the right vertical structure (satisfies the J08 data).
3. We find the self-consistent equilibrium of our chosen dark halo in the presence of the bulge, the gas disc and our adopted double-exponential stellar disc.
4. By adjusting masses and radial scale(s) of the double-exponential disc (and consequently of the gas disc, which is tied to the stellar disc), we seek satisfaction of the constraints on $v_\mathrm{c}(R)$ listed in Section 2 – these comprise the terminal velocities and data for the masers and Sgr A*. Each time the the disc parameters are changed, we relax the halo again in the presence of the updated disc. Thus after each unsuccessful comparison with data of the rotation curve generated by the dark-halo DF in the presence of the current double-exponential disc, we return to step 2.
5. We choose a DF for the stellar disc that has the scale lengths found in Step 4 and we adopt plausible values for the velocity-dispersion parameters.
6. Then we determine a new overall potential as follows. (i) We update the contribution of the disc to the density that generates the potential to the density obtained by integrating the disc DF over velocities using the current estimate of the potential. (ii) We solve for the potential generated by the updated disc density and the current estimate of the dark-halo density. (iii) We update the contribution of the dark halo to the density that generates the potential to the density obtained by integrating the halo DF over velocities in the current potential. (iv) We again solve for the overall potential. Then we return to step (i) until the updates become insignificant.
7. With the potential frozen at its current value, we adjust the velocity-dispersion parameters in the disc DF to obtain a good fit of the model's kinematics to the kinematics of the RAVE giants in eight spatial bins. At this stage we include the contribution of the stellar halo with its DF normalised as described in Section 3.2. Then we return to Step 6 and follow it with Step 7 until updates become negligible.
8. We compute the residuals between the vertical stellar density profile of J08 and that implied by the DFs of the disc and stellar halo.
9. If these residuals are unsatisfactory, we choose a new mass for the dark halo and return to Step 2.

This algorithm derives from two physical principles. First the predicted rotation curve is sensitive to the scale lengths of the disc components and insensitive to the velocity dispersion parameters. Second the velocity-dispersion parameters control the kinematics of stars within each spatial bin with little sensitivity to the potential used. Consequently, even when the potential employed is far from the truth, the RAVE data yield values for the velocity-dispersion parameters that are close to the final best-fit values. Given the value of σ_{z0}, the correct potential can be identified by comparing the density profile predicted by the DF to the star-count data.

Replacing the double-exponential discs by the density distribution generated by the disc DF in step 6 changes the potential very little. We do not include the stellar halo in the sources of the gravitational potential because its mass should be negligible, even though the mass implied by our DF can be significant depending on its ill-constrained behaviour at small actions that do not contribute to the RAVE data. Because the density distribution generated by the disc DF is not *exactly* the same as that generating the dummy potential, it is not practical to set the DF normalisation such that we obtain the same total mass as generates the dummy potential. Instead we normalise such that the disc DF yields the same radial force at the Sun as does the dummy potential.

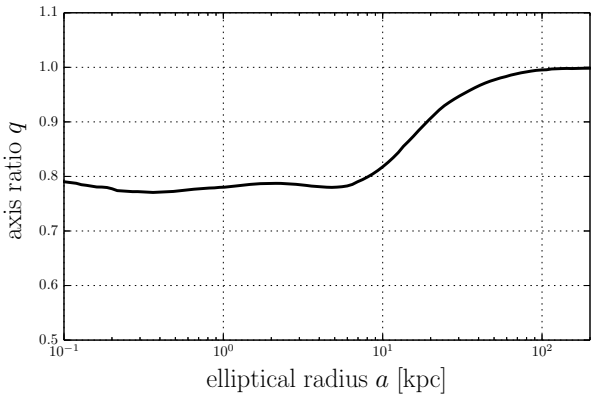

Figure 1. The axis ratio q of the final dark halo as a function of semi-major axis length a.

5 RESULTS

Here we describe our best-fit model. Table 3 gives the values of the parameters in the final dark halo's DF, and below the line some derived properties. Its local density is

$$\rho_{\rm DM}(R_0, 0) = 0.01307\,{\rm M}_\odot\,{\rm pc}^{-3} = 0.50\,{\rm GeV\,cm}^{-3}. \quad (20)$$

In the absence of the discs and bulge, the DF of the dark halo generates a spherical mass distribution. Fig. 1 shows the final dark halo's axis ratio q as a function of semi-major axis length a. At $a \lesssim R_0$ the axis ratio is fairly constant at just below 0.8, and then, as the influence of the disc wanes, it increases towards $q = 1$, implying spherical symmetry. The axis ratio $q \simeq 0.8$ in the inner Galaxy is consistent with the findings of PPB, but their halo became rounder sooner because their disc was more compact.

For the halo scale action J_0 we find a value around $6000\,{\rm km\,s^{-1}\,kpc}$. This parameter is, however, only weakly constrained by our data and strongly correlated with the derived halo virial mass because the latter is largely determined by the density of the dark halo well outside R_0, while our data constrain the halo density at $r \lesssim R_0$. In fact, the virial mass of the dark halo can be increased without much impact on our data by increasing J_0 so the density within R_0 changes little. Taken in isolation, i.e. used to recover the dark halo's structure before the baryons fell in, our dark-halo DF yields an NFW profile that has scale length $r_s \simeq 16\,{\rm kpc}$, virial radius $R_{200} = 223\,{\rm kpc}$, and virial mass $M_{200} = 1.4 \times 10^{12}\,{\rm M}_\odot$.

The stellar discs have a scale length $R_{\rm d} = 3.66\,{\rm kpc}$ and total mass $3.6 \times 10^{10}\,{\rm M}_\odot$. At R_0 the stellar surface density is $46.3\,{\rm M}_\odot\,{\rm pc}^{-2}$. The total baryonic mass (i.e., including the Bulge and the gas disc) is $6.2 \times 10^{10}\,{\rm M}_\odot$. Hence we have a (visible) baryon fraction of 4.2 per cent. The remaining parameters of the disc DF are given in Table 2.

In the upper panel Fig. 2 we show the final model's circular speed $v_{\rm c}(R)$. For comparison we added in blue $v_{\rm c}(R)$ for the model of P14 with $q = 0.8$. The curves are very similar except for the region $R \lesssim 3\,{\rm kpc}$ in which circular orbits are impossible on account of the Galactic bar. Consequently, the model is unconstrained in this region. The grey curves in this panel show circular speeds that are generated by the dark matter (full curve) and baryons (dashed curve). The lower panel of Fig. 2 shows the ratio of the radial forces coming from the baryons and dark matter. On account of adiabatic contraction, our model contains much more dark matter at small radii than that of P14. At the Sun the ratio, 0.61, is even lower than that, 0.85, of P14, so only 38 per cent of the radial force on the Sun is due to baryons. Moreover, whereas in the P14 model the contribution to F_R from baryons rises steeply inwards, becoming dominant at $R \lesssim 5\,{\rm kpc}$, in the present model it remains low until $R \simeq 3\,{\rm kpc}$ and the baryons are dominant only at $R \lesssim 2\,{\rm kpc}$.

Table 2. Parameters of the stellar disc DF. All parameters were adjusted when fitting the data.

Parameter	value	unit
Σ_0	110	${\rm M}_\odot\,{\rm pc}^{-2}$
$R_{\rm D}$	3.66	kpc
Thin disc		
$\sigma_{R,{\rm thn}}$	35.40	${\rm km\,s^{-1}}$
$\sigma_{z,{\rm thn}}$	26.00	${\rm km\,s^{-1}}$
$R_{\sigma_R,{\rm thn}}$	$2R_{\rm d}$	
$R_{\sigma_z,{\rm thn}}$	$2R_{\rm d}$	
Thick disc		
$\sigma_{R,{\rm thk}}$	52.78	${\rm km\,s^{-1}}$
$\sigma_{z,{\rm thk}}$	53.33	${\rm km\,s^{-1}}$
$R_{\sigma_R,{\rm thk}}$	11.6	kpc
$R_{\sigma_z,{\rm thk}}$	5.01	kpc
$F_{\rm thk}$	0.416	

Table 3. Parameters of the dark halo's DF. Of these parameters, only N was adjusted when fitting the data. R_{200} and M_{200} are derived parameters of the dark halo that is generated by the DF in the absence of other components.

Parameter	value	unit
N	8.825×10^{12}	${\rm M}_\odot$
$h_{\rm max}$	10^6	${\rm km\,s^{-1}\,kpc}$
J_0	6000	${\rm km\,s^{-1}\,kpc}$
$J_{\rm core}$	1.25×10^{-2}	${\rm km\,s^{-1}\,kpc}$
R_{200}	223	kpc
M_{200}	1.4×10^{12}	${\rm M}_\odot$

Fig. 3 compares the vertical stellar density profile above the Sun with the star count data from J08. The model star density comprises that predicted by the disc DF plus that predicted by the DF of the stellar halo when normalised as described in Section 3.2. The agreement between model and data is excellent.

Fig. 4 shows our fit to the kinematics of RAVE giants in the four spatial bins that lie inside R_0: the coordinates of the barycentre of each bin are given at the bottom of the centre panel of each row. The fits are excellent apart from a deficit of almost non-rotating stars that becomes more marked as one moves away from the plane. This deficit points to weakness in our choice of DF for the stellar halo and/or the thick disc.

The black curve in Fig. 5 shows the vertical gravitational force K_z in the solar cylinder as a function of distance from the Galactic plane, z. The brown and blue curves show force laws computed from Bovy & Tremaine (2012) and P14,

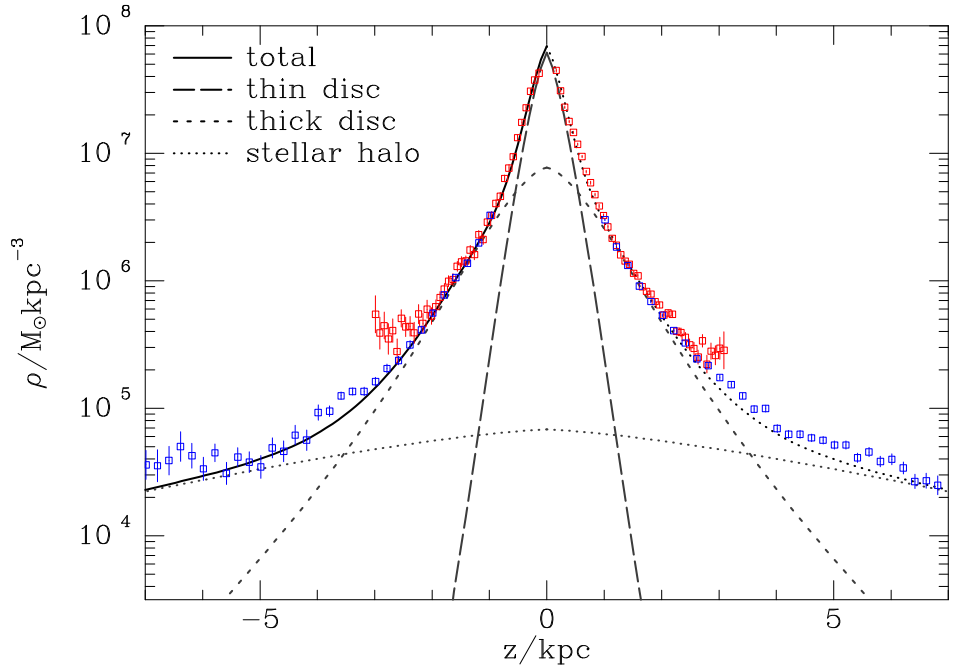

Figure 3. Vertical stellar density profiles in the solar annulus of our composite model (solid line), the thin disc (dashed line) and the thick disc (dotted line), and the stellar halo (dotted line). The red and blue error bars show the data from Jurić et al. (2008). Only the

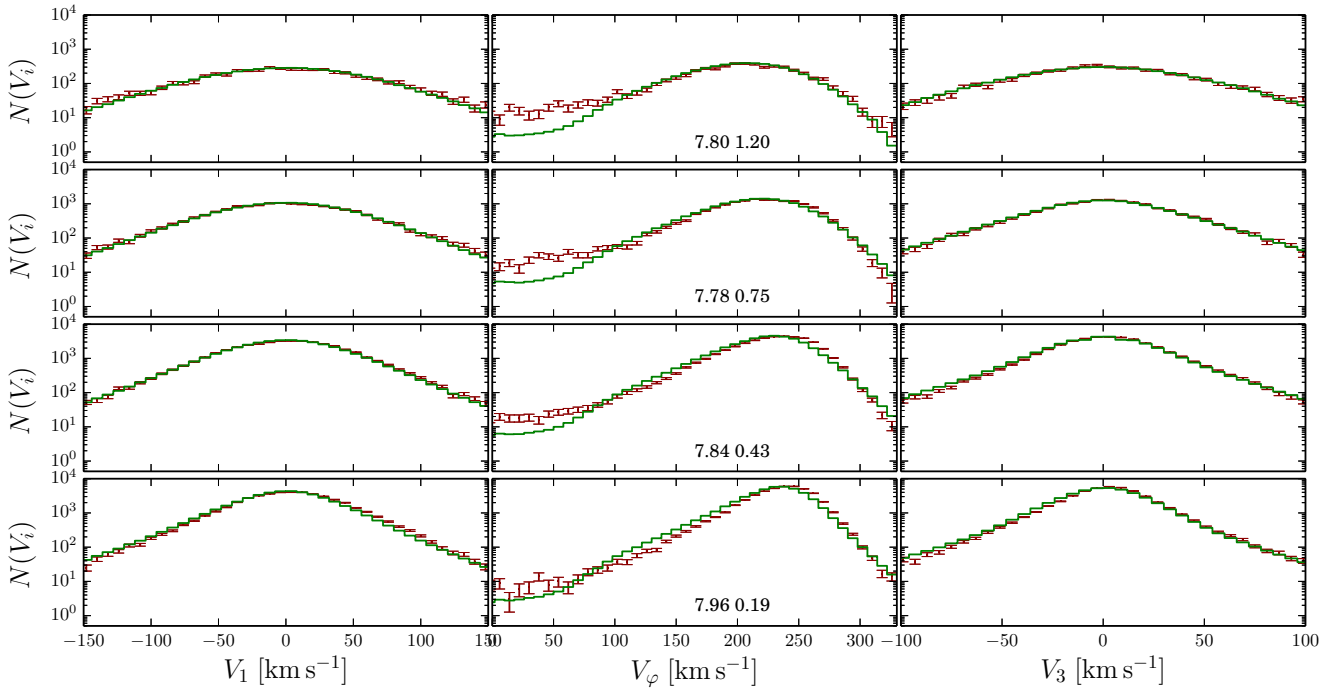

Figure 4. Model (green curves) and observed (red error bars) velocity distributions for RAVE giants with $R_0 - 1\,\mathrm{kpc} < R < R_0$. Each row represents a slice in distance from the Galactic plane. The (R, z) coordinates of the barycentre of the stars in each slice are given in the middle panels. These are also the locations where the DF was evaluated. A correction described in PPB was applied to the model prediction to incorporate the influence of errors in the measurement of both velocities and distances.

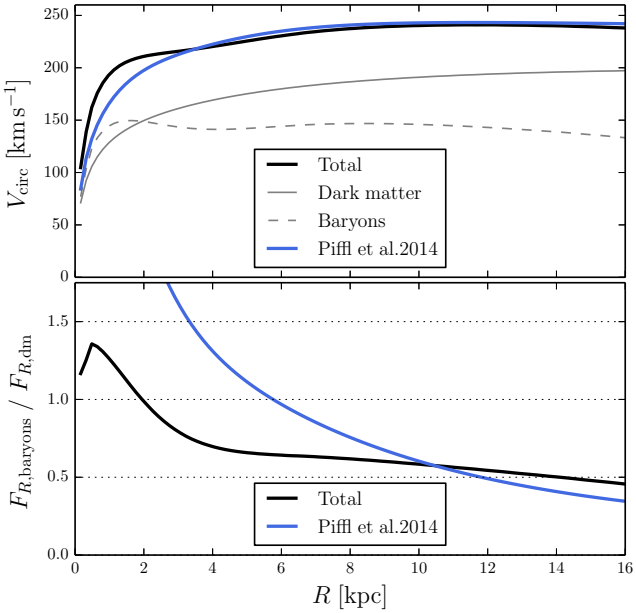

Figure 2. Upper panel: $v_{\rm c}(R)$ for our final Galaxy model (black lines) and, for comparison, for the P14 model (blue lines). The solid lines show the total $v_{\rm c}$, while the dashed and dotted lines show the contributions of the dark halo and the baryons, respectively. Lower panel: the ratio of the radial forces stemming from the baryonic components and the dark matter halo for our model and the P14 model.

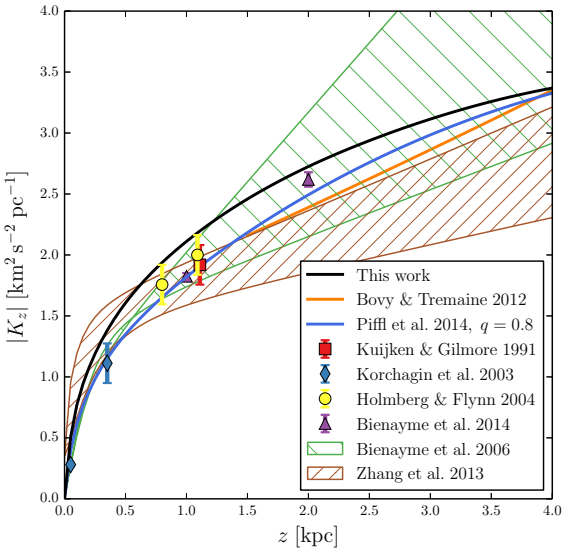

Figure 5. Vertical force $|K_z|$ in the solar cylinder as a function of distance z from the Galactic plane. See the main text for a further discussion

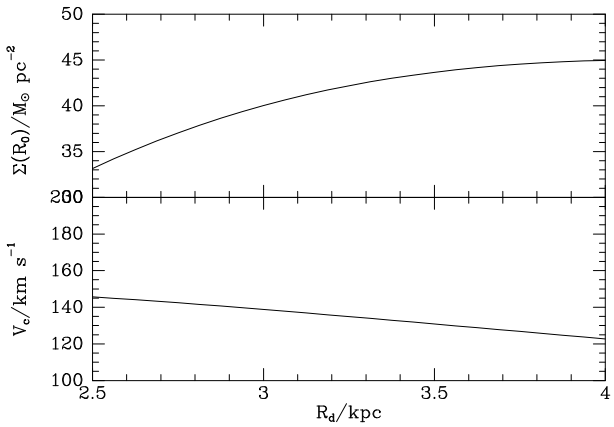

Figure 6. Lower panel: contribution to $v_{\rm c}(R_0)$ from a thin exponential disc with mass $M_{\rm disc} = 3.6 \times 10^{10}\,{\rm M}_\odot$ and varying scale lengths. Upper panel, the surface density of such a disc at R_0.

respectively, the blue curve being that for the P14's model with $q = 0.8$. Error bars show results from a number of other studies, including the seminal work of Kuijken & Gilmore (1991). Only Korchagin et al. (2003), Bienaymé et al. (2006) and P14 constrain K_z significantly at $|z| < 1\,$kpc. In general there is good agreement between the studies.

Even though our disc is slightly less massive than that of P14 (3.6 rather than $3.7\times10^{10}\,{\rm M}_\odot$), it generates larger K_z at all z because its longer scale length implies a higher surface density at the Sun (46.3 rather than $37.1\,{\rm M}_\odot\,{\rm pc}^{-2}$). In fact, its high local surface density ensures that at all values of z its K_z exceeds that from other studies.

6 DISCUSSION

By replacing the fixed NFW dark halo used by P14 with a dynamically active dark halo, one increases the ratio of dark-halo densities, $\rho_{\rm DM}(3\,{\rm kpc})/\rho_{\rm DM}(R_0)$. Since the value of $\rho_{\rm DM}(R_0)$ is strongly constrained by solar neighbourhood data – which leave no doubt that the disc can contribute only part of $v_{\rm c}(R_0)$ – the tendency encountered by PPB for a more centrally concentrated dark halo to drive $v_{\rm c}(3\,{\rm kpc})$ above the observational limits must be addressed by increasing the scale length of the disc. If done at fixed disc mass, this operation moves disc material outwards, thus counteracting the increased central concentration of the dark halo on its becoming active. However, as the lower panel of Fig. 6 shows, increasing $R_{\rm d}$ at fixed disc mass reduces the disc's contribution to $v_{\rm c}(R_0)$. Hence there is little scope for reducing either $M_{\rm disc}$ or $\rho_{\rm DM}(R_0)$ below the values found by P14. The upper panel of Fig. 6 shows that as $R_{\rm d}$ is increased at fixed $M_{\rm disc}$, the local stellar surface density $\Sigma(R_0)$ increases. The scope for such an increase is limited by the RAVE and J08 data. Hence the present optimisation process leads to a model with a longer disc scale length but similar mass and $\rho_{\rm DM}(R_0)$. Pressure from the constraints on $v_{\rm c}(3\,{\rm kpc})$ drives the disc to higher values of $\Sigma(R_0)$ and K_z than are ideal from the perspective of the RAVE and J08 data.

6.1 Constraints from microlensing

Above we found a model with an adiabatically compressed dark halo that is consistent with all the observational constraints of Section 2. However, we now show that this model is not consistent with data not so far considered, namely the measured optical depth to microlensing of bulge stars. Binney & Evans (2001) took the local density of dark matter to be $\rho_{\rm DM}(R_0) = (0.0136 \pm 0.007)\,{\rm M}_\odot\,{\rm pc}^{-3}$ in close agree-

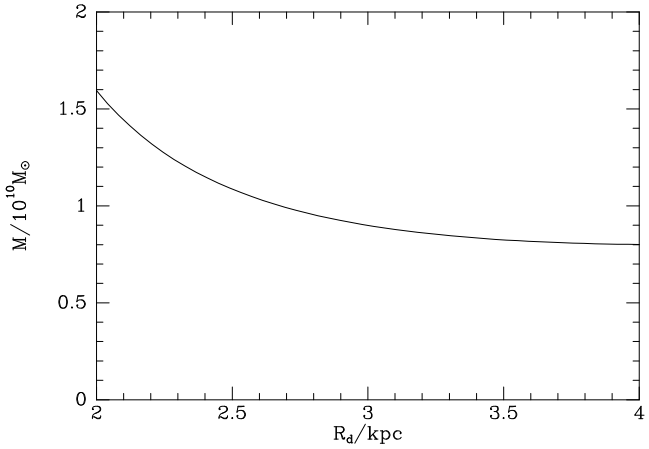

Figure 7. Mass as a function of scale length for a thin exponential disc that contributes a given amount, $10\,\mathrm{M}_\odot\,\mathrm{pc}^{-2}$, to the local surface density.

ment with our value. For any adopted value of the local dark-matter density, the local surface density of the baryonic disc followed from the measured total surface density $\Sigma_0 = 71 \pm 6\,\mathrm{M}_\odot\,\mathrm{pc}^{-2}$ within 1.1 kpc of the plane (Kuijken & Gilmore 1991). Binney & Evans assumed that the baryons were arranged in such a way, as regards the ellipticity of the bar and the scale height of the disc, that the optical depth to microlensing along the line of sight ($l = 0, |b| \simeq 4^\circ$) was maximised for any given contribution to v_c. Taking the optical depth on this line of sight to be at least 2×10^{-6} (Popowski et al. 2005), and extrapolating the adopted local dark-matter density inwards as a power law of slope $-\alpha$, they showed that the inferred values of v_c exceeded those implied by measurements of tangent velocities unless α was significantly smaller than unity or $\rho_\mathrm{DM}(R_0) < 0.007\,\mathrm{M}_\odot\,\mathrm{pc}^{-3}$. Our adiabatically compressed dark halo has $\rho_\mathrm{DM}(R_0) = 0.014$ and $\alpha > 1$, so it comfortably violates these constraints.

6.2 Are long disc scale lengths viable?

To simplify the fitting process, we set the scale lengths of the thin and thick discs equal, and obtained $R_\mathrm{d} = 3.66\,\mathrm{kpc}$. This value is in good agreement with that obtained for the thin disc from SEGUE data by Bovy et al. (2012). It is also consistent with the long scale length ($R_\mathrm{d} = 3.6\,\mathrm{kpc}$) J08 measured for the thick disc.

However, the thick disc is now generally distinguished from the thin disc by high values of the abundance of α elements such as Mg relative to Fe at a given value of [Fe/H]. When the thick disc is defined thus, current data suggest that the thick disc has a shorter scale length than the thin disc (Hayden et al. 2015; Recio-Blanco et al. 2014; Nissen & Schuster 2014), contrary to the finding of J08. If the thick disc does have a short scale length, this will have a significant impact on the viability of the current model, because the model assigns significant mass to the thick disc ($1.06 \times 10^{10}\,\mathrm{M}_\odot$). The vertical density profile of J08 essentially fixes the contribution of the thick disc to the local surface density. Fig. 7 shows as a function of scale length the mass of an exponential disc that contributes $10\,\mathrm{M}_\odot\,\mathrm{pc}^{-2}$ to the local surface density. It shows that shortening the scale length of the thick disc will make it more massive. Its peak contribution to v_c will be increased by both this increase in its mass and the shortening of its scale length. Moreover, any increase in the central density of the thick disc will further compress the dark halo and further increase v_c. Hence, it seems unlikely that there is significant scope for reducing the scale length of the thick disc without violating the constraints of Section 2.

There are indications that the chemically defined, low-α abundance, thin disc is flared (Minchev et al. 2015). This being so, our geometrically thick disc with a long scale length may be consistent with a short scale length for the α-enhanced thick disc. Consequently, the requirement for a large scale length is not as serious an issue as the requirement for a higher optical depth to microlensing.

6.3 Selection functions

An aspect of the present work which should be improved, is the neglect of selection functions. Any survey captures only a fraction of the stars that exist within any volume. The fraction that is captured varies with distance, and with intrinsic stellar properties such as mass, chemistry and age, that determine the star's absolute magnitudes in the relevant wavebands. The stellar densities from J08 on which we have relied take fully into account the selection function of the SDSS photometric survey. In comparing the kinematics predicted by models with the RAVE data we should properly have considered biases towards younger or older stars, since the age of a star affects its likely kinematics. Sanders & Binney (2015) explored the impact of accounting for age biases on the best-fitting parameters of DFs of the present type in the context of GCS data. This exercise has not yet been performed for RAVE data, but it should be. We doubt that proper treatment of age biases would materially affect the conclusions we have reached here.

7 CONCLUSIONS

We have extended the approach of PPB from the construction of a single Galaxy model in which both the stellar disc and the dark halo are represented by distribution functions in the the self-consistently generated gravitational potential to a systematic search through a multi-dimensional parameter space of such models. As in the model of PPB the dark halo has the structure expected if the baryons fell in smoothly, so the dark matter was adiabatically compressed. Consequently, the dark halo is more centrally concentrated than the NFW profile, which arises in simulations of cosmological clustering of dark matter only.

Whereas the model of PPB violated the observational constraints on $v_\mathrm{c}(R)$ at $R < R_0$, our search of parameter space has identified a model that is consistent with these constraints. The secret to achieving consistency is an increase in the scale length of the disc at essentially fixed stellar mass. The derived disc scale length, $R_\mathrm{d} = 3.66\,\mathrm{kpc}$, may be acceptable for the thin disc, but it is probably unacceptably large for the thick disc. However, our work suggests that a model with an adiabatically compressed dark halo in which the thick disc has a realistically short scale length can-

not be made consistent with the constraints on v_c at small radii.

Since dark matter does not cause microlensing and the model assigns to the dark halo much of the overall density at small radii, it violates by some margin the constraints on the dark halo that Binney & Evans (2001) deduced from the microlensing data.

Hence by ruling out adiabatic compression this study furnishes compelling evidence that there has been a significant transfer of energy from the baryons to the dark halo. Such a transfer has been proposed by many authors because it can arise through drag on the bar (Tremaine & Weinberg 1984; Sellwood 2008), drag on molecular clouds (Nipoti & Binney 2015), energy injection by supernovae (Mashchenko et al. 2008), and by cosmic infall (Johansson et al. 2009; Goerdt et al. 2010).

Given that we can now exclude adiabatic compression of the dark halo, the natural next step is to impose priors on the scale lengths of the thin and thick discs derived from spectroscopic studies of Galactic chemistry, and to add the microlensing data to the constraints listed in Section 2. Then one should use the fitting procedure developed here to build self-consistent models using DFs for the dark halo that imply increasing extents of central heating of dark matter by baryons. In this way it should be possible to place a lower limit on extent of dark-matter heating. We hope to publish the results of such a study in the near future.

ACKNOWLEDGEMENTS

The research leading to these results has received funding from the European Research Council under the European Union's Seventh Framework Programme (FP7/2007-2013)/ERC grant agreement no. 321067.

Funding for RAVE has been provided by: the Australian Astronomical Observatory; the Leibniz-Institut für Astrophysik Potsdam (AIP); the Australian National University; the Australian Research Council; the French National Research Agency; the German Research Foundation (SPP 1177 and SFB 881); the European Research Council (ERC-StG 240271 Galactica); the Istituto Nazionale di Astrofisica at Padova; The Johns Hopkins University; the National Science Foundation of the USA (AST-0908326); the W. M. Keck foundation; the Macquarie University; the Netherlands Research School for Astronomy; the Natural Sciences and Engineering Research Council of Canada; the Slovenian Research Agency; the Swiss National Science Foundation; the Science & Technology Facilities Council of the UK; Opticon; Strasbourg Observatory; and the Universities of Groningen, Heidelberg and Sydney. The RAVE web site is at http://www.rave-survey.org.

REFERENCES

Aumer M., Binney J. J., 2009, MNRAS, 397, 1286
Bienaymé O., Soubiran C., Mishenina T. V., Kovtyukh V. V., Siebert A., 2006, A&A, 446, 933
Binney J., 2010, MNRAS, 401, 2318
Binney J., 2011, Pramana, 77, 39
Binney J., 2012, MNRAS, 426, 1328
Binney J., McMillan P., 2011, MNRAS, 413, 1889
Binney J., Merrifield M., 1998, Galactic Astronomy. Princeton University Press
Binney J., Tremaine S., 2008, Galactic Dynamics: Second Edition. Princeton University Press
Binney J., Gerhard O., Spergel D., 1997, MNRAS, 288, 365
Binney J. et al., 2014, MNRAS, 439, 1231
Binney J. J., Evans N. W., 2001, MNRAS, 327, L27
Bissantz N., Gerhard O., 2002, MNRAS, 330, 591
Bovy J., Tremaine S., 2012, ApJ, 756, 89
Bovy J., Rix H. W., Liu C., Hogg D. W., Beers T. C., Lee Y. S., 2012, ApJ, 753, 148
Casagrande L., Schönrich R., Asplund M., Cassisi S., Ram´irez I., Meléndez J., Bensby T., Feltzing S., 2011, A&A, 530, A138
Dehnen W., Binney J., 1998, MNRAS, 294, 429
Flynn C., Holmberg J., Portinari L., Fuchs B., Jahreiß H., 2006, MNRAS, 372, 1149
Gillessen S., Eisenhauer F., Fritz T. K., Bartko H., Dodds-Eden K., Pfuhl O., Ott T., Genzel R., 2009, ApJ, 707, L114
Goerdt T., Moore B., Read J. I., Stadel J., 2010, ApJ, 725, 1707
Hayden M. R. et al., 2015, ArXiv e-prints
Holmberg J., Nordström B., Andersen J., 2007, A&A, 475, 519
Johansson P. H., Naab T., Ostriker J. P., 2009, ApJ, 697, L38
Jurić M. et al., 2008, ApJ, 673, 864
Korchagin V. I., Girard T. M., Borkova T. V., Dinescu D. I., van Altena W. F., 2003, AJ, 126, 2896
Kordopatis G. et al., 2013, AJ, 146, 134
Kuijken K., Gilmore G., 1991, ApJ, 367, L9
Malhotra S., 1995, ApJ, 448, 138
Mashchenko S., Wadsley J., Couchman H. M. P., 2008, Science, 319, 174
McMillan P. J., 2011, MNRAS, 414, 2446
McMillan P. J., Binney J. J., 2010, MNRAS, 402, 934
Minchev I., Martig M., Streich D., Scannapieco C., de Jong R. S., Steinmetz M., 2015, ApJ, 804, L9
Navarro J. F., Frenk C. S., White S. D. M., 1997, ApJ, 490, 493
Nipoti C., Binney J., 2015, MNRAS, 446, 1820
Nissen P. E., Schuster W. J., 2014, in S. Feltzing, G. Zhao, N.A. Walton, P. Whitelock, eds, IAU Symposium. IAU Symposium, Vol. 298, pp. 65–70
Nordström B. et al., 2004, A&A, 418, 989
Piffl T., Penoyre Z., Binney J., 2015, ArXiv e-prints
Piffl T. et al., 2014, MNRAS, 445, 3133
Popowski P. et al., 2005, ApJ, 631, 879
Posti L., Binney J., Nipoti C., Ciotti L., 2015, MNRAS, 447, 3060
Recio-Blanco A. et al., 2014, A&A, 567, A5
Reid M. J., Brunthaler A., 2004, ApJ, 616, 872
Reid M. J. et al., 2014, ApJ, 783, 130
Sanders J. L., Binney J., 2015, ArXiv e-prints
Schönrich R., 2012, MNRAS, 427, 274
Schönrich R., Binney J., Dehnen W., 2010, MNRAS, 403, 1829
Sellwood J. A., 2008, ApJ, 679, 379
Steinmetz M. et al., 2006, AJ, 132, 1645
Tremaine S., Weinberg M. D., 1984, MNRAS, 209, 729

van der Kruit P. C., Searle L., 1981, A&A, 95, 105
van der Kruit P. C., Shostak G. S., 1984, A&A, 134, 258
Yanny B. et al., 2009, AJ, 137, 4377